Simulating Underexpanded Plumes in Martian and Lunar Environments

Thomas P. Shurtz[1]
Jacobs Space Exploration Group, Huntsville, AL, 35806, USA

Jeffrey S. West[2]
NASA Marshall Space Flight Center, Huntsville, AL, 35808, USA

While the Loci/Chem Computational fluid dynamics (CFD) application has been validated and used extensively for simulating launch environments in atmospheric conditions, use of this tool for simulating supersonic plumes at much lower ambient pressure requires further validation. Simulations of underexpanded plumes have been performed using Loci/Chem at Martian pressure to predict several metrics for laminar, turbulent, and impinging plumes. The CFD results are compared with an experimental data set for low Reynolds number plumes at these conditions in order to evaluate the current capability of the Loci/Chem tool for these types of environments. The CFD validation results to date show reasonable agreement with the experimental data across all the metrics of interest for the configurations considered. The Loci/Chem-Boltzmann tool is a hybrid continuum/rarefied flow solver which extends modeling capabilities to very low-pressure environments such as those on the Moon. The Loci/Chem-Boltzmann solver uses a gradient-based continuum breakdown criterion to restrict solution of the computationally expensive Boltzmann equation to only a subset of the domain, while using the Navier-Stokes equations elsewhere. This CFD application is und`er active development, and current efforts toward establishing production ready capability for evaluating Lunar plume surface interactions are well under way. Initial simulations of an Apollo Lunar excursion module indicate that several regions of the flow require solving the Boltzmann equations due to extreme rarefaction. Early simulations are promising, indicating reasonable overall computational time for a full 3D human scale lander simulation.

I. Nomenclature

D_m	=	diameter of Mach disk
P	=	pressure
P_0	=	stagnation / plenum pressure
P_a	=	ambient pressure
Re_{exit}	=	Reynolds number defined by nozzle exit properties
S_f	=	fluorescence signal
T	=	temperature
T_0	=	stagnation / plenum temperature
w	=	primary wavelength
X_{NO}	=	nitric oxide concentration
$x_{fully\ trans}$	=	relative axial location of transition to turbulence
$x_{fully\ turb}$	=	relative axial location of fully developed turbulence
$x_{unsteady}$	=	relative axial location of onset of unsteadiness
x_m	=	relative axial location of Mach disk

[1] Fluid Dynamicist, Propulsion Systems Support.
[2] Technical Assistant, Fluid Dynamics Branch ER42.

II. Introduction

The complex physical phenomena that occur during a propulsive vehicle descent include plume surface interactions (PSI). PSI is an active area of research and modeling. With a renewed focus on returning humans to the Moon and then on to Mars it is expected that PSI computational modeling and simulation in low pressure atmospheres will be needed to provide metrics influencing critical design decisions.

A project focused on improving understanding and modeling capability of PSI was recently awarded by the NASA Space Technology Mission Directorate (STMD) Game Changing Development (GCD) program. A primary element of the project is to enhance computational predictive capabilities. The predictive simulation capability (PSC) development element is divided into four tasks: (1) simulating plume structure in low-pressure environments, (2) simulating crater development and ejecta, (3) regolith particle phase modeling, and (4) gas-particle interaction modeling. As part of the task 1 effort to bring computational tools and methods to production readiness in predicting low pressure plume behavior, it is necessary to evaluate the capabilities of existing toolsets.

Current computational fluid dynamics (CFD) tools have been verified and validated for a wide range of applications in earth atmosphere where they are regularly applied. However, for extraterrestrial landing applications, simulations in low pressure atmospheres will be needed. The validation envelope must be extended to include environments such as Mars atmosphere and Lunar near vacuum.

This paper describes the activities and accomplishments to date for the component of the PSC element focusing on validating existing tools for use in simulating plumes in both Martian and Lunar low-pressure environments. The validation plan for the PSC element describes and calls for both an initial, approximate, baseline validation assessment, as well as a more rigorous detailed validation assessment [1]. The existing Loci/Chem tool has been previously validated and is regularly used for launch vehicle applications where ambient conditions model Earth's atmosphere [2]-[5]. This Navier-Stokes flow solver is expected to be suitable for simulating plumes in Martian atmosphere, where pressures, although much lower than Earth atmosphere, support a continuum fluid assumption. A baseline validation assessment of the Loci/Chem tool for simulating plumes in Martian environments has been completed by comparing simulation results to a select few experimental cases. Detailed validation of Loci/Chem for simulating plumes at Martian conditions has begun, by simulating a wider set of conditions across a parametric space. The results of this completed baseline validation, and the ongoing detailed validation efforts are described here.

For simulations of flows in rarified conditions where the continuum assumption does not hold, a Navier-Stokes solver is expected to be insufficient to accurately model certain behavior. The Loci/Chem-Boltzmann tool is a hybrid continuum/rarified flow solver that uses the discretized Navier-Stokes equations in appropriate regions of the flow and uses the discretized Boltzmann equations in non-continuum regions of the flow [6]. The tool makes use of a continuum breakdown criteria to dynamically switch between Boltzmann and Navier-Stokes solvers on a cell by cell basis to maximize efficiency, and only use the computationally expensive Boltzmann solver in cells where the Navier Stokes solutions would not be accurate. While this tool is still in active development, it is the capability of choice for simulating plumes in Lunar environments. Before a baseline validation assessment of the tool is practical, it is necessary to demonstrate that it can be used for production-like cases. Such a demonstration, simulating an Apollo lander, is described in this paper.

III. Simulations of Plumes in Martian Environments

The baseline validation assessment task described in the PSC validation plan requires that the predictive capabilities of the existing Loci/Chem tool be compared to a subset of experimental cases described in Jennifer Inman's doctoral dissertation [7]. The detailed validation assessment plan adds to the rigor of validation by expanding comparison to additional cases from the Inman dataset, as well as additional datasets that will become available through testing performed as part of the GCD PSI project. The initial validation assessment has been completed by comparing the results of Loci/Chem simulations to three cases from the Inman dataset, each of which is characterized by distinctive conditions and behavior [8]. The detailed validation assessment has begun, by simulating an additional six cases from Inman's data. These additional cases cover a range of Reynolds numbers, with other conditions being held constant from case to case.

A. Experimental Dataset Used for Comparison

The experimental dataset generated by Jennifer Inman was created to make available a high quality CFD validation resource for low pressure / low Reynolds number plumes. Because of the low pressure environment, Planar Laser Induced Florescence (PLIF) was used as a visualization technique to capture imagery of plumes over a range of Reynolds numbers and pressure ratios. An example image produced by the PLIF technique is shown in Fig. 1.

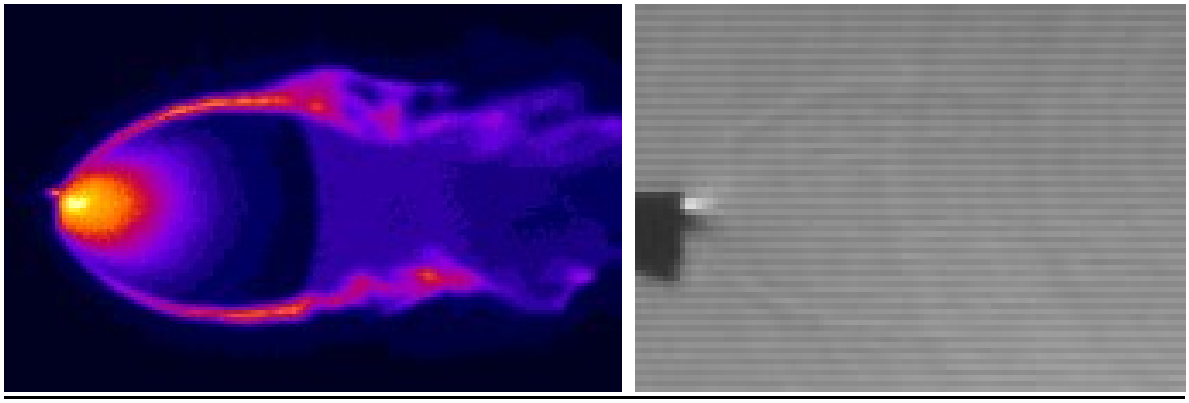


Fig. 1 Representative images produced by different visualization techniques applied to a low-pressure plume: Nitric Oxide PLIF (left), and Schlieren (right). From [7].

The test hardware consisted of a heated steel plenum and nozzle inside a vacuum chamber test section. The plenum was fed and pressurized with a mixture of 99.5% N2 and 0.5% NO gas, which was heated and accelerated through the nozzle, and exhausted into the vacuum chamber. The plenum itself was heated by electrical heat tape wrapped around the model. Gas temperatures were not finely controlled but were measured in the plenum with a thermocouple. Plenum pressure was measured with a pressure transducer. The exit diameter was only varied by selecting either a fixed sonic nozzle with exit diameter of 0.095 inches, or a fixed supersonic nozzle with exit diameter of 0.164 inches. A diagram of the experimental apparatus setup is shown in Fig. 2.

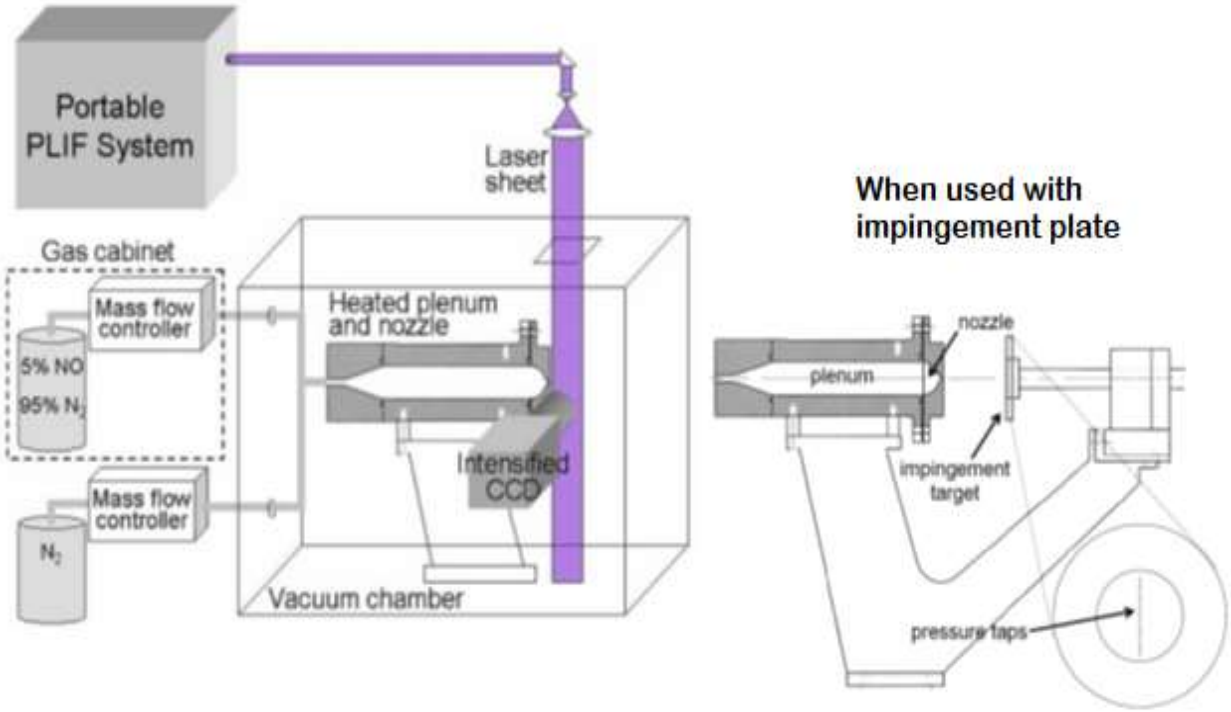


Fig. 2 Diagram of experimental apparatus used by Inman [7].

Experiments included both sonic and supersonic plumes, with and without an impingement surface. A subset of three cases was chosen which includes both laminar and turbulent plumes from a sonic nozzle, and a laminar impinging

plume from a supersonic nozzle. The parameters of interest were varied in the experiment by independently controlling the list of variables shown in Table 1. The combination of these parameters, along with the presence or absence of an impingement plate, determined the plume type shown in the far left column of Table 1.

Table 1 Parameters varied in Inman experiments

	Independently Varied			Derived	
Parameter	T_0	P_0	P_a	$Pressure\ Ratio$	Re_{exit}
Steady Free	590 K	6.95 kPa	133 Pa	27.6	1,116
Turbulent Free	527 K	23.9 kPa	3201 Pa	3.9	4,386
Impinging	514 K	22.84 kPa	222 Pa	5.4	2,302

Output from the experiment consisted of PLIF images of the plumes, and in cases with impingement, pressures at a series of tap locations. The PLIF images were processed and analyzed to generate a series of quantitative output metrics. A list of the dependent variables reported for the experiments is shown in Table 2. A subset of the output metrics was recorded for each configuration of the input parameters. However, no single configuration includes details for all the metrics in Table 2. The three cases chosen for the baseline validation include each of the plume types, and therefore collectively include all the reported metrics.

Table 2 Dependent variables output from experiment

Type of Case	Metric of interest	Description
Laminar non-impinging plumes	x_m	Axial distance from nozzle exit plane to Mach disk
	D_m	Diameter of Mach disk
	w	Primary wavelength. Axial distance between nozzle exit plane and location where reflected barrel shock intersects the plume boundary
Turbulent non-impinging plumes	$x_{unsteady}$	Axial distance between nozzle exit and location at which unsteadiness in the shear layer is first observed
	$x_{fully\ trans}$	Axial distance between nozzle exit and location at which all of the plume, including the core, exhibits transitional behavior
	$x_{fully\ turb}$	Axial distance between nozzle exit and location at which turbulence is fully developed and all spatial modes are active
Impinging plumes	P	Pressure distribution across impingement target as measured at tap locations

The metrics reported for the laminar plume cases in the experiment were defined in terms of identifiable shock structure features in the PLIF imagery as shown in Fig. 3. The single case chosen for the baseline validation assessment of the laminar, non-impinging plume type was designated as Run 78 in Inman's dissertation. The reported shock structure parameters were determined by the experimenters viewing the PLIF images of the plumes in the camera software program WinView32. They recorded the location of a given feature in terms of the pixel location within the image. The pixel locations were then converted to physical dimensions by using images of a ruler scale taken with the same camera system. The image resolutions were typically about 180 pixels/inch, resulting in a lower bound on uncertainty of ±2.8 thousandths of an inch, or 3% of nozzle diameter. The reported metrics for Run 78 are listed with corresponding values in Table 3.

Table 3 Output metrics recorded for laminar plume experimental Run 78

Metric	x_m	D_m	w
Value	0.4869 inches	0.2122 inches	0.5631 inches

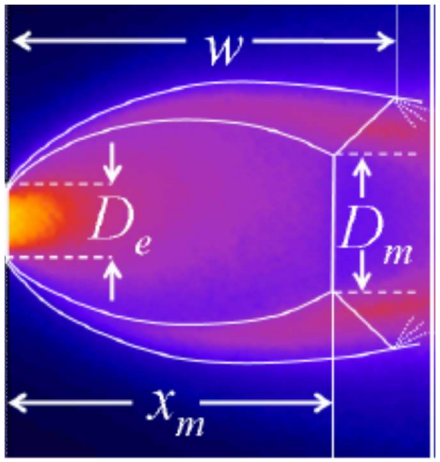


Fig. 3 Shock structure metrics reported for laminar plume cases [7].

The metrics reported for the turbulent plume cases in the experiment were defined in terms of laminar to turbulent transition along the axial direction aligned with the plume flow as shown in Fig. 4. The single case chosen for the baseline validation assessment of the turbulent, non-impinging plume type was designated as Run 32 in Inman's dissertation. For the turbulent plume cases, 100 images were captured over a 10s period. The images were smoothed, processed to remove background noise, and normalized to account for varying laser intensity. The standard deviation of pixel brightness was calculated for the set of images, and a smoothing filter was applied to the result. This smoothed standard deviation image had a colormap applied and was then visually inspected to determine the metrics, which were marked on the colormap image by the experimentalists. The selection criteria, metric definition, and inspecting personnel changed throughout the course of the experimental data generation. The image with marked metrics for Run 32 was included in Iman's dissertation. Pixel density puts a lower bound on uncertainty of ± 3% of a nozzle diameter. The values of the metrics as determined from the image with included scale are shown in Table 4.

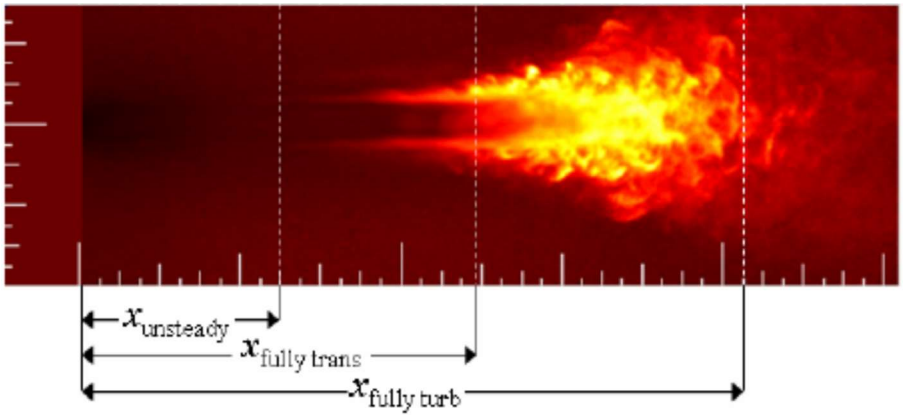


Fig. 4 Unsteady turbulent plume metrics reported for experimental Run 32 [7]

Table 4 Unsteady turbulent plume metrics as determined from image in Fig. 4

Parameter	$x_{unsteady}$	$x_{fully\ trans}$	$x_{fully\ turb}$
Value	0.61(5) inches	1.23(3) inches	2.06(8) inches

The only quantitative output metric for the impinging plume configurations is the pressure distribution recorded at 32 tap locations on an impingement target. The 1 Hz sampled pressure at each tap was averaged over a duration of approximately 10 seconds (10 samples). This mean pressure at each tap was recorded on a spreadsheet which includes

markings indicating that some of the pressure tap measurements were discarded. The single case chosen for baseline validation of the impinging plume type was designated Run 536 in Inman's dissertation. The pressure distribution reported for Run 536 is shown in plot form in Fig. 5

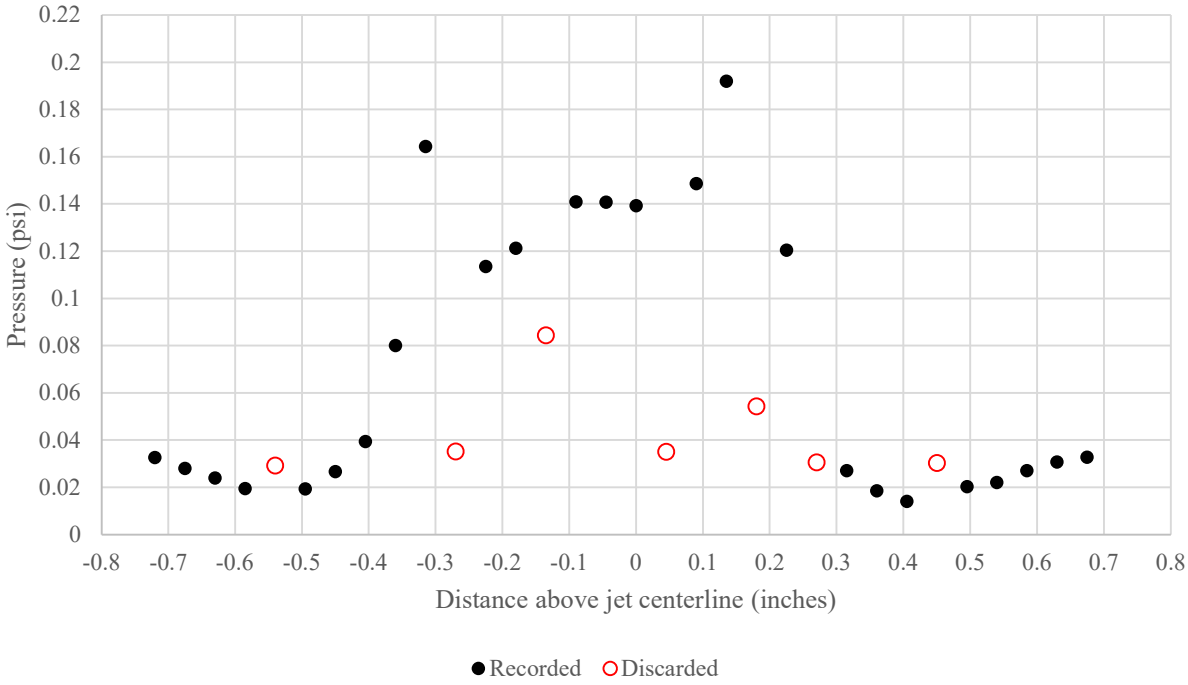


Fig. 5 Impingement pressure distribution reported for experimental Run 536 [7]

B. Simulation Methodology

The baseline validation simulations were intended to assess the current capability of Loci/Chem for simulating plumes at Martian-like conditions using a typical production approach. This meant targeting an approach which would allow for approximately a three-week turnaround time to produce initial results after getting geometry from a customer. Solver settings were not adapted specifically to improve performance or accuracy for any one configuration. Rather, the settings were chosen in such a way that a wide parametric set of cases could be run with simple adjustments to the prescribed boundary conditions. The methods chosen allow for robust operation of the code with relatively fast completion. Computation time for a single configuration requires about 12 hours on 2,016 Broadwell processors (72 nodes) at the NASA Advanced Supercomputing (NAS) facility.

1. Geometry, Boundary Conditions, and Mesh

The model geometry of the simulations was constructed to approximate the experimental apparatus for the plenum, nozzle, and the impingement plate (impinging plume case only). The apparatus tunnel walls were not included in the simulations. Instead, far field boundaries were placed far (50+ nozzle diameters radially) from the nozzle exit. The cylindrical boundaries allow for incoming entrainment flow, while the downstream outflow boundary assumes flow out of the domain. The simulations for non-impinging plumes make use of the same geometry and boundary condition types as shown in Fig. 6. The "Farfield" and "Outflow" pressure values were varied to match the ambient conditions of the respective experiments. The inflow conditions were varied to match the respective total flow conditions in the plenum for each experiment. The geometry and boundary conditions used for the impinging plume simulation are shown in Fig. 7.

The simulations make use of unstructured meshes to discretize the domain. The meshes are not particularly adapted to the specific flow conditions for the cases simulated but are designed to be used for any set of flow conditions across the full range of Inman's experiments. The mesh is refined in the region of the nozzle lip (~0.003 nozzle diameter edge length), and slowly grows to larger cells (geometric expansion factor of 1.05) toward the far field boundaries as shown in Fig. 8 and Fig. 9. The entire mesh for the impinging plume cases is approximately 100 million cells, while the mesh for the impinging plume case is approximately 150 million cells. The larger cell count for the impinging

plume mesh is due to refinement near the impingement place, and a more extensive region of refinement in the nozzle due to the longer supersonic nozzle geometry.

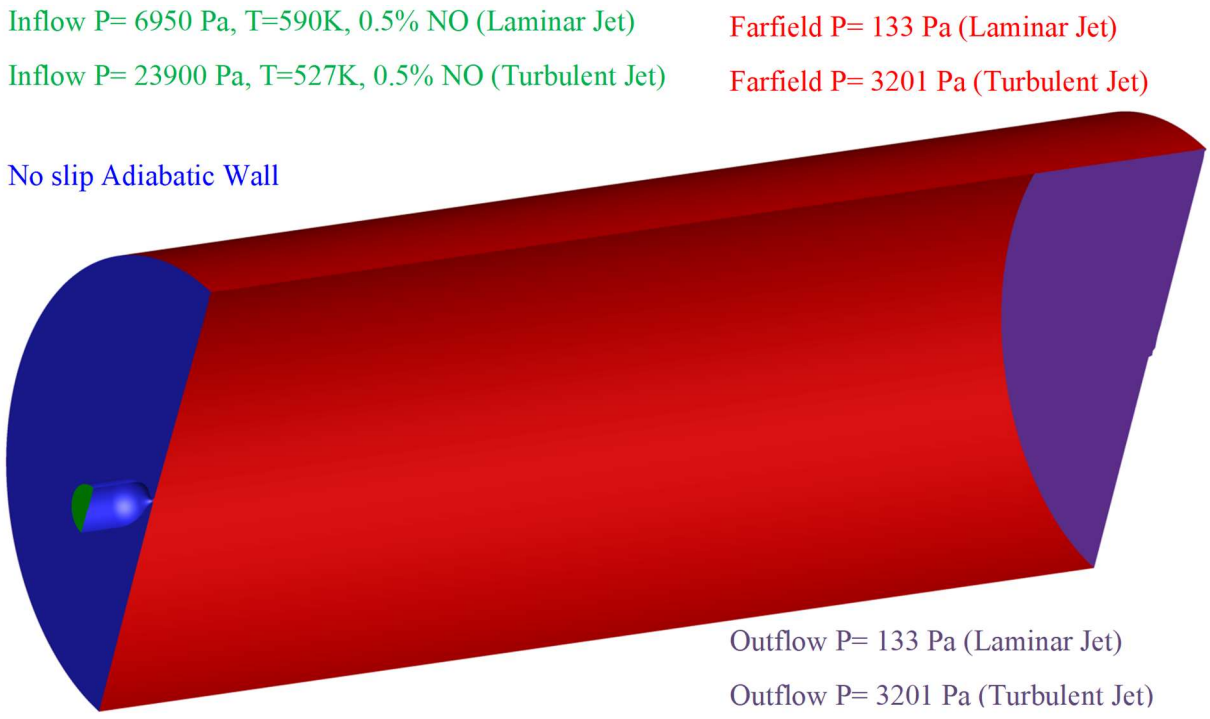


Fig. 6 Geometry and boundary conditions specified in non-impinging plume simulations

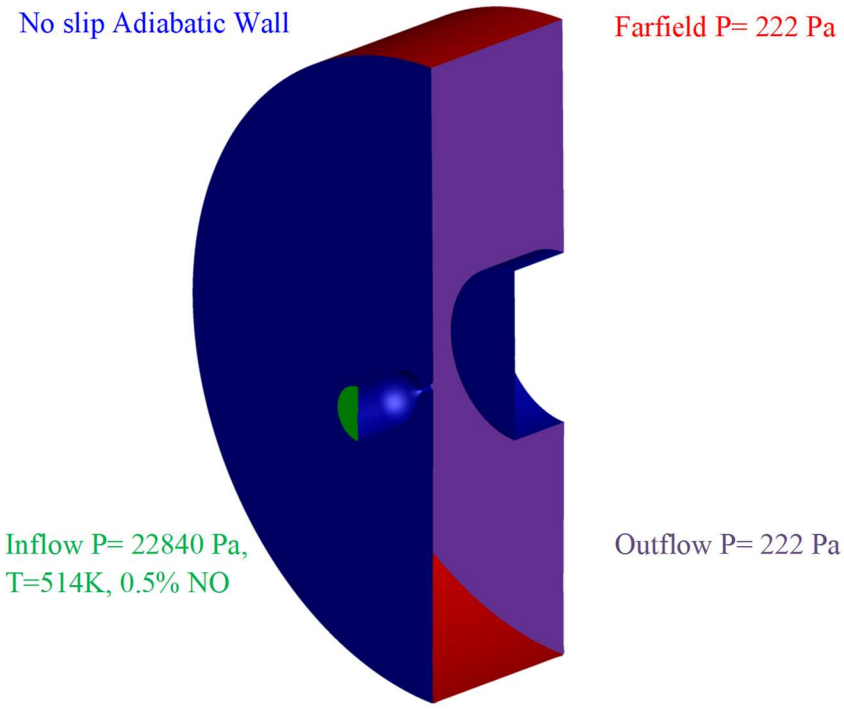


Fig. 7 Geometry and boundary conditions specified for impinging plume simulation

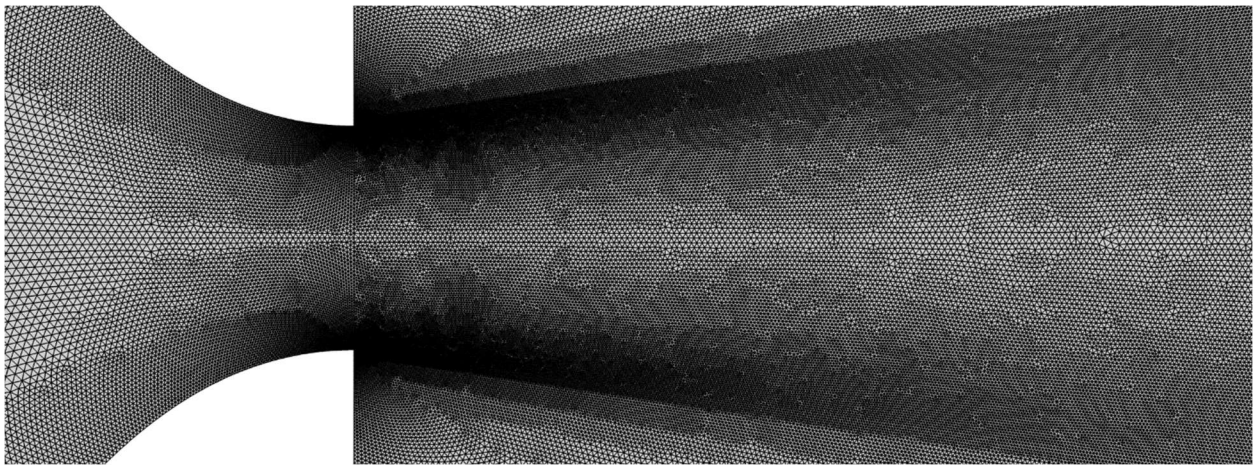


Fig. 8 Mesh detail near nozzle lip for non-impinging plume cases (Run 78 and 32)

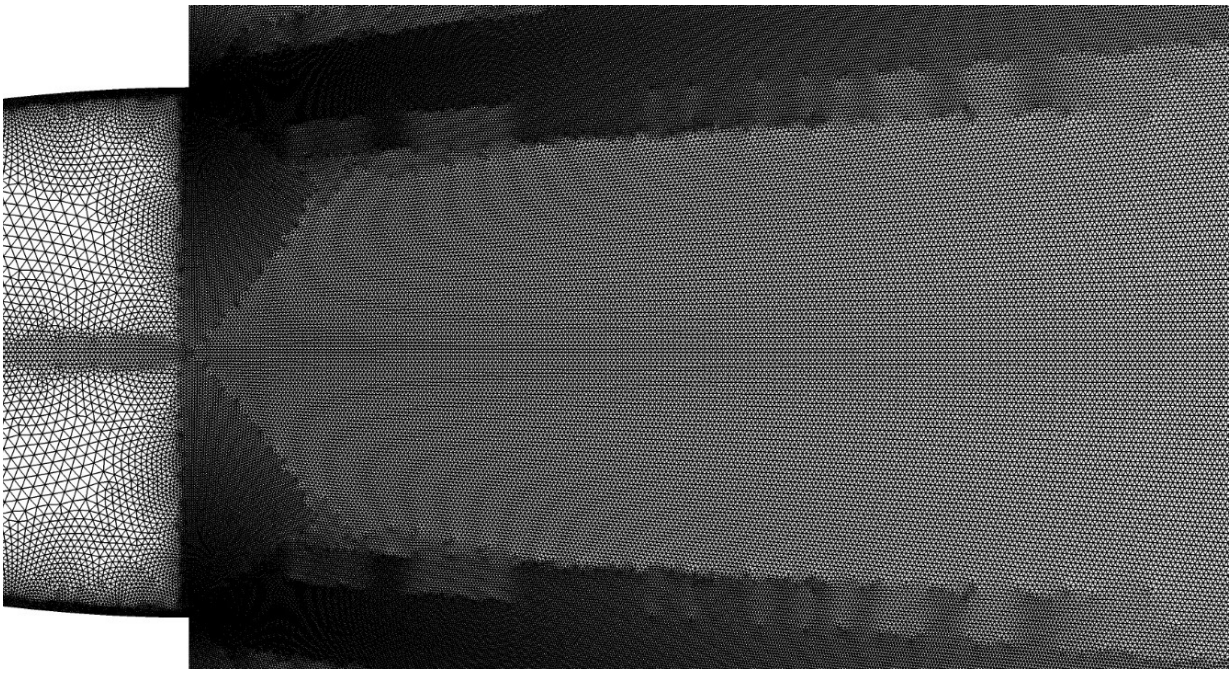


Fig. 9 Mesh detail near nozzle lip for supersonic impinging case (Run 536)

2. Quantitative metric extraction

Direct, qualitative comparison of the experimental dataset to the computational simulations is difficult, due to the inherent differences in the way metrics were obtained from the experiments, and the possible methods by which they can be extracted from the CFD solutions. However, a repeatable, objective methodology for extracting metrics from the simulation results has been defined for use in both baseline and detailed validation assessments. This methodology is applied to a statistical reduction of the time-accurate CFD solution results calculated using 100 snapshots taken at intervals of 100 timesteps.

For the laminar plume CFD that corresponds to experimental Run 78, an isocontour of mean Mach number = 1 is used to define the shock structure metrics. The intersection of the Mach 1 isocontour and the jet centerline defines the location of the Mach disk and the length x_m. The width of the inner contour (subsonic bubble) defines the diameter of the Mach disk D_m. The axial location of the pinch point in the outer contour defines the primary wavelength w.

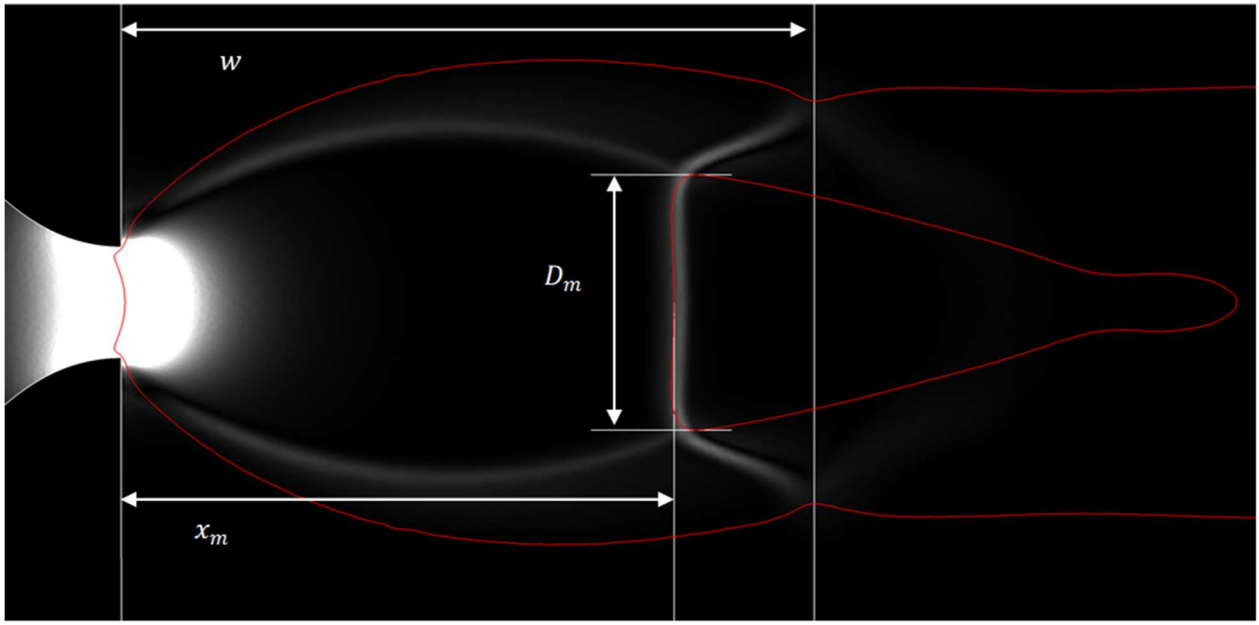


Fig. 10 Definition of shock structure metrics from CFD solution for laminar plume. Background image includes grayscale pressure gradient contour overlaid with red Mach 1 isocontour

The turbulent transition metrics for the non-impinging turbulent plume are defined in terms of the resolved turbulent kinetic energy (TKE). The resolved TKE is half the sum of the variances of the three velocity components as calculated during statistical reduction of the time accurate solution. A contour plot of TKE for a turbulent plume is shown in Fig. 11, overlaid with a red contour at 10% of the peak centerline value. The turbulent transition metrics are defined in terms of this 10% contour as shown.

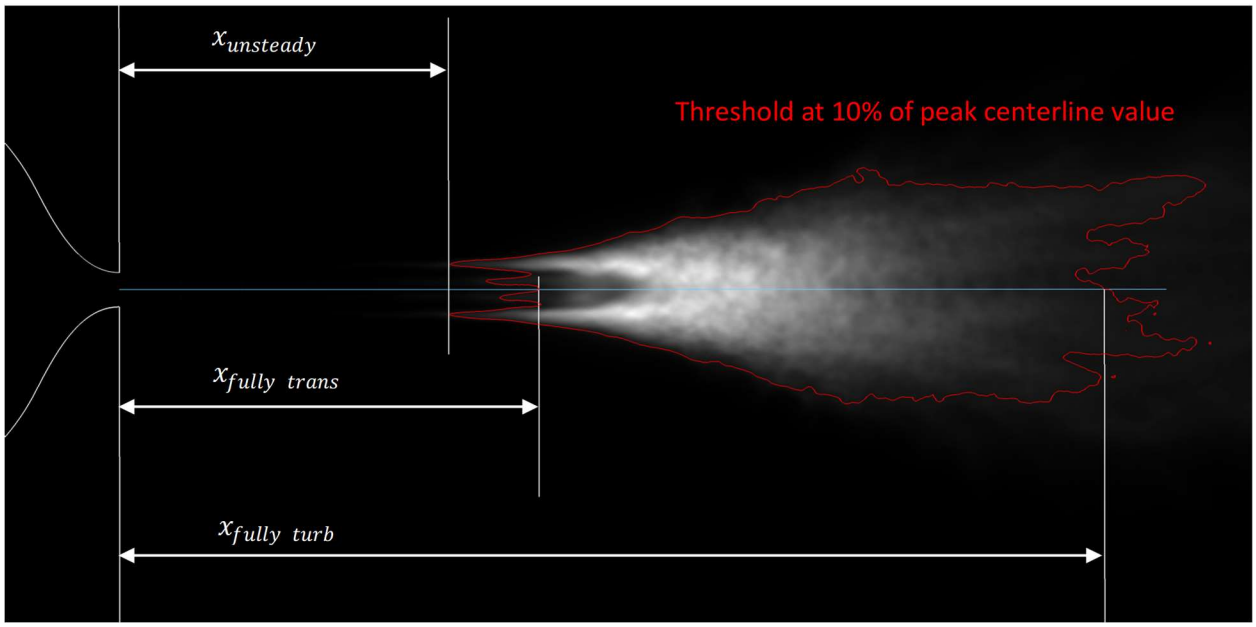


Fig. 11 Definition of turbulent transition metrics from CFD solution for turbulent plume

The static impingement pressure is the only qunatitative metric that needs to be extracted from the CFD solution of the impinging plume case. This is rather straightforward. The static pressure is simply extracted along a line defined by the intersection of a plane cutting through the center of the geometry (and plume) and the impingement plate surface as shown in Fig. 12. The impingement pressures are then available at each mesh point along this line.

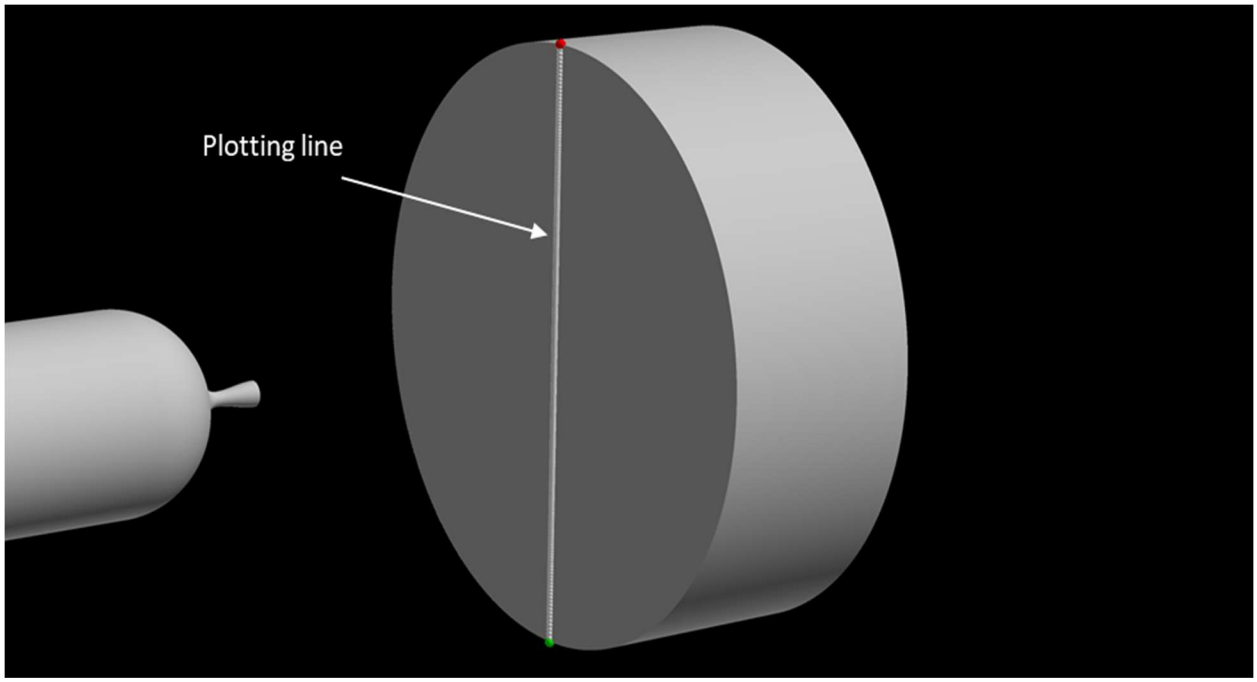


Fig. 12 Location of impingement pressure extraction from CFD solution for impinging plume

C. Comparison of Results

The CFD simulation metrics obtained using the processes described above can be directly compared to the metrics reported for the experiments. A side by side comparison of the CFD solution for the non-impinging laminar plume and the PLIF from experimental Run 78 is shown in Fig. 13. The CFD solution (shown on left) is visualized with contours of the magnitude of the pressure gradient. The feature locations for extracted metrics are overlaid on this image for both CFD results (green) and the experimental observations (magenta). The experimental PLIF image (shown on right) has the same feature locations overlaid (CFD in green and experiment in magenta).

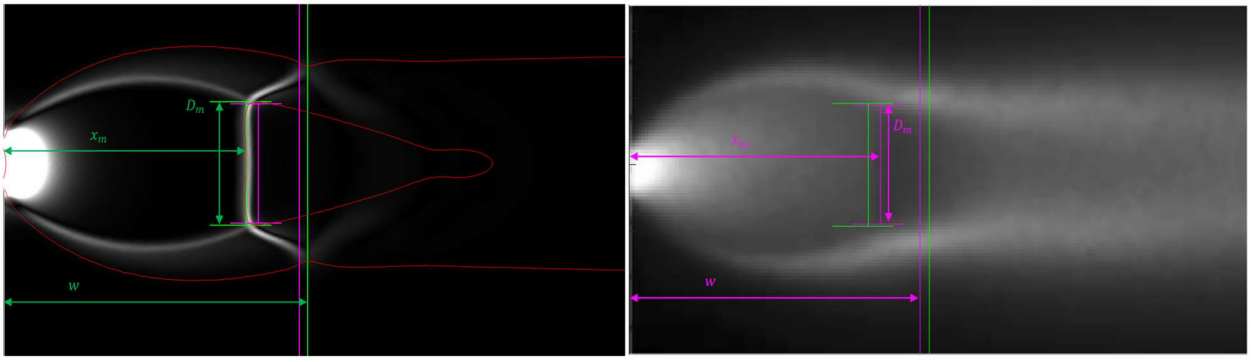


Fig. 13 Side by side comparison of laminar plume CFD results to experimental PLIF. Left: CFD results colored by pressure gradient magnitude. Right: experimental Run 78 PLIF [7]. Metrics from CFD are shown in green, while metrics from experiment are shown in magenta

A similar side by side comparison of the CFD solution for the turbulent plume to the experimental Run 32 is shown in Fig. 14, with the CFD solution visualized on the left by contours of TKE. The feature locations for extracted metrics are overlaid for both CFD results (green) and the experimental observations (magenta). The standard deviation of PLIF data from the experiment is shown on the right with CFD metrics overlaid in green and experimentalist observed metrics in magenta. Despite the subjective manner in which the metrics were extracted from the experiment, the overall unsteady features of the jet occur in similar locations in both the experiment and CFD results.

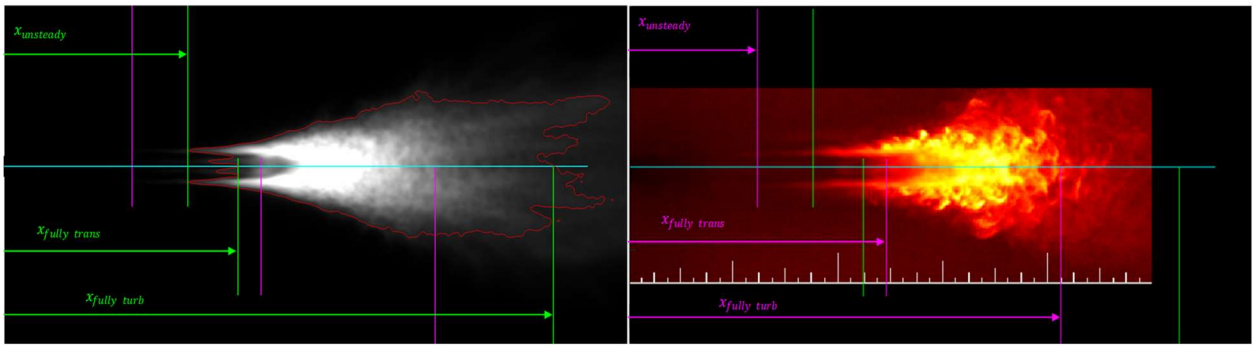


Fig. 14 Side by side comparison of turbulent plume CFD results and experimental PLIF. Left: CFD results colored by TKE. Right: colorized standard deviation of Run 32 PLIF [7]. Metrics from CFD are shown in green, while metrics from experiment are shown in magenta

A side by side qualitative comparison of the impinging plume CFD results to the experimental PLIF is shown in Fig. 15. The CFD results are visualized on the left using a computational flow imaging technique that approximates PLIF brightness [9], while the experimental PLIF is shown on the right. Although plume structure metrics for this case were not extracted for either the experiment or the simulation, the qualitative similarity is striking.

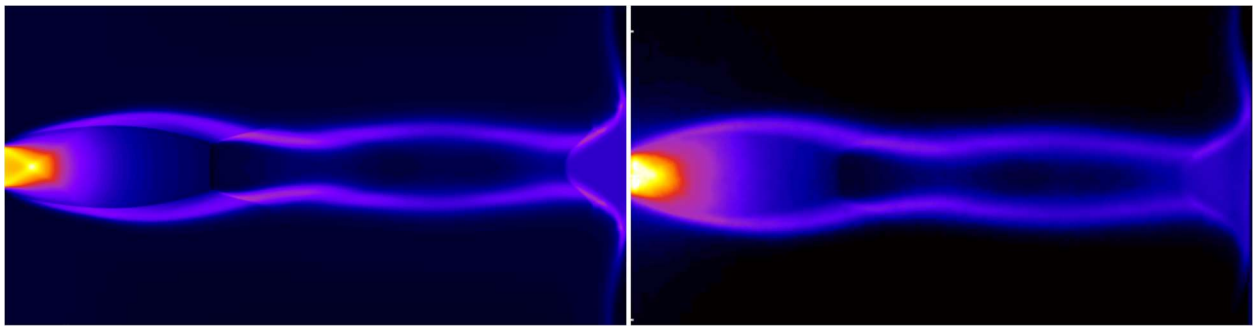


Fig. 15 Side by side comparison of impinging plume CFD results to experimental PLIF. Left: CFD results colored by temperature. Right: colorized PLIF from experimental Run 536 [7]

The impingement pressure distribution for the CFD and corresponding experiment are shown in an overlaid plot in Fig. 16. The experimental results are slightly asymmetrical (skewed to the left on the plot) do to slightly off-center impingement. The overall shape of the pressure distribution as predicted by the simulation is similar to the experimental results, with the primary discrepancy being an overpredicted plateau pressure and peak pressure.

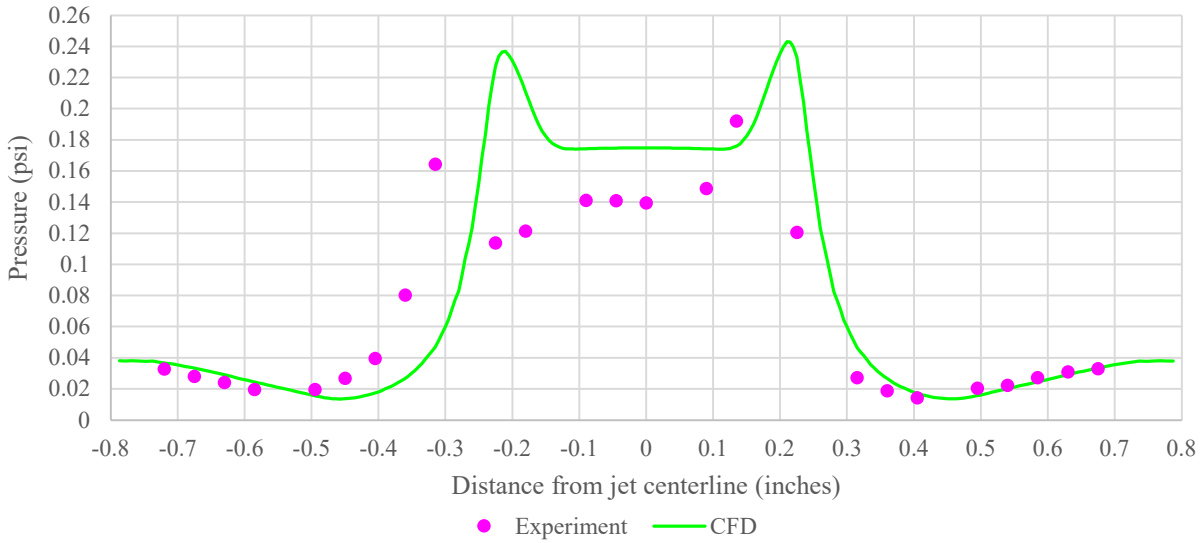


Fig. 16 Comparison of impinging plume CFD predicted impingement pressure to experimental Run 536

The GCD PSC validation plan specifies a target threshold value (indicating usefulness for production work) of +/- 25% for plume structure metrics at Martian ambient conditions. A tabulated summary comparison of all metrics for the Martian plume baseline validation assessment is shown in Table 5. All shock structure metrics for laminar plumes are predicted with 5% of experimental values. Turbulent transition metrics are much more subjective in nature, and CFD predictions vary as much as 44%. The primary metric of interest for this validation effort, which directly impact PSI phenomena is impingement pressure. The CFD simulations predict the impingement pressure plateau within 24% of the experiment.

Table 5 Tabulated comparison of all metrics from runs 78, 32, and 536 used for baseline validation

Metric of interest	Experiment	CFD	% Difference
x_m	0.4869 inches	0.4635 inches	-4.8%
D_m	0.2122 inches	0.2197 inches	+3.5%
w	0.5631 inches	0.5811 inches	+3.2%
$x_{unsteady}$	0.615 inches	0.8881 inches	+44%
$x_{fully\ trans}$	1.233 inches	1.1220 inches	-9.0%
$x_{fully\ turb}$	2.068 inches	2.6350 inches	+27%
P (plateau)	0.141 psi	0.1747 psi	+24%

D. Initial Detailed Validation Assessment Activities

A detailed validation assessment is intended to raise the level of rigor beyond that of the baseline assessment and provided more informative evaluations of Loci/Chem capabilities for simulating plumes in Martian environments. It includes several aspects which increase both the breadth and depth of comparison to experimental data. One of these aspects is to cover a wider range of the Inman dataset, including parametric spaces in Reynolds number, pressure ratio, and impingement distance. Initial efforts at a detailed validation assessment have begun, exploring a parametric Reynolds number space at constant pressure ratio. A side by side qualitative comparison of CFD results to experiment for plumes with Reynolds numbers ranging from 1500 to 36000 is shown in Fig. 17 and Fig. 18.

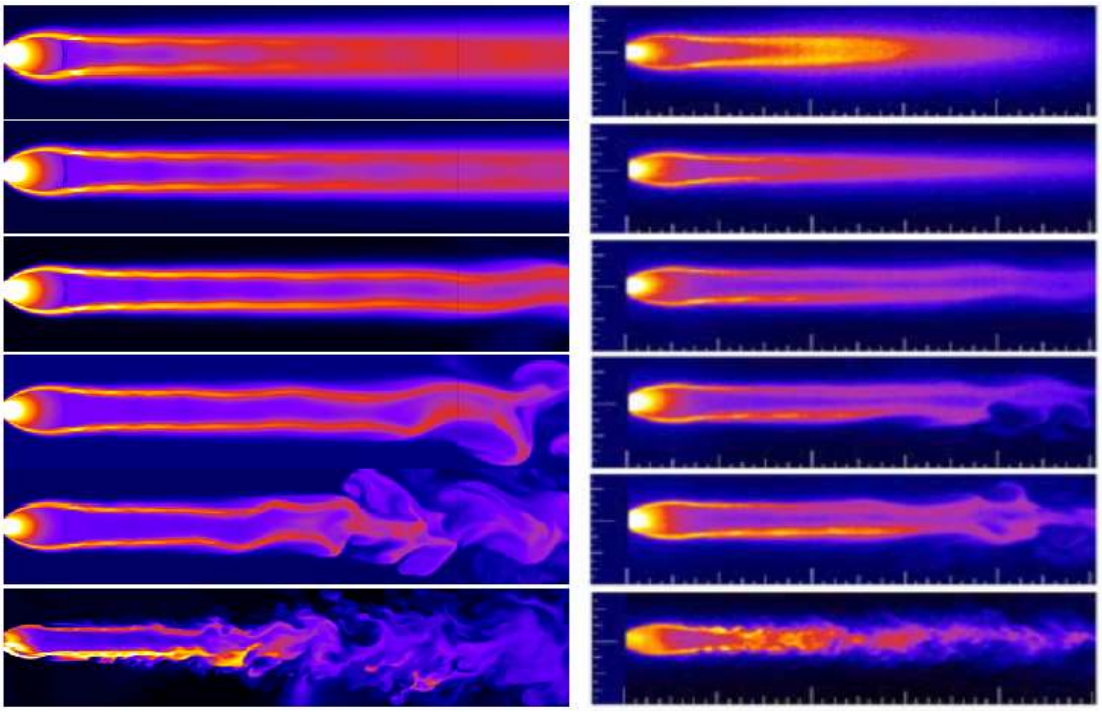


Fig. 17 Side by side comparison of instantaneous CFD (left) to experimental PLIF(right) [7] for a range of Reynolds numbers. From top to bottom: Re = 1500, 2700, 4400, 5500, 6600, 36000. Respective experimental runs 9, 60, 35, 38, 34, and 71

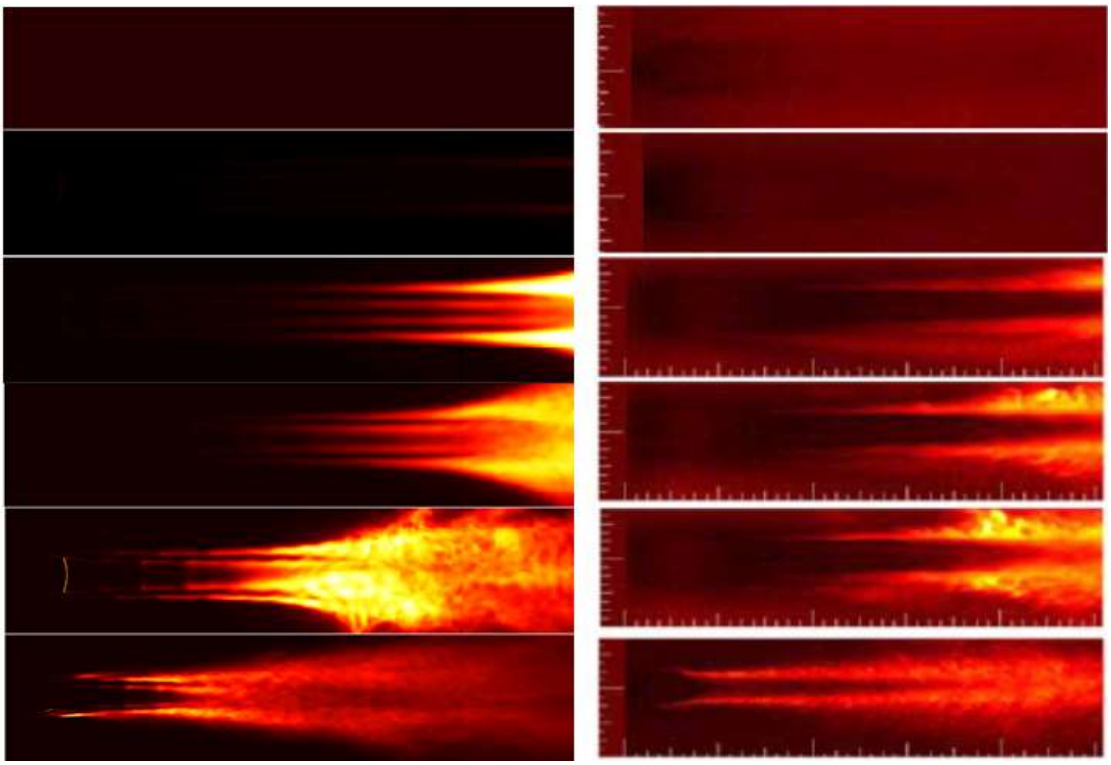


Fig. 18 Side by side comparison of standard deviation of CFD simulated PLIF (left) [7] to experimental PLIF(right) for a range of Reynolds numbers. From top to bottom: Re = 1500, 2700, 4400, 5500, 6600, 36000. Respective experimental runs 9, 60, 35, 38, 34, and 71

This initial qualitative comparison indicates the Loci/Chem code is capturing certain trends in physical behavior of plumes with respect to Reynolds number. The transition location shifts upstream and the instantaneous solutions contain smaller scale fluctuations as Reynolds number increases. These results are promising, and more in depth and quantitative validation efforts will continue as part of the detailed validation plan.

E. Summary of Activities and Accomplishments

To date, the use of Loci/Chem for simulating plumes in Martian environments has now been demonstrated as practical using a production type approach, with generic mesh suitable for a range of input parameters. A baseline validation assessment has been made by quantitatively comparing the CFD results to Inman's experimental data for a minimal set of three cases covering all reported metrics. The simulations were able to predict impingement pressure within 24% of the experiment, indicating threshold capability target is met for the existing tool without additional development. Detailed validation assessment of Loci/Chem for simulating plumes in Martian environments has begun, and initial results are promising. Loci/Chem simulations capture trends in plume turbulent structure with increasing Reynolds number. As detailed assessment efforts continue, the envelope of validation will be expanded to include low-pressure continuum environments, allowing confident use of the tool for predicting PSI relevant environments for customers.

IV. Simulating Plumes in Near Vacuum Lunar Environments

This section describes efforts to demonstrate production ready capability of the Loci/Chem-Boltzmann solver to simulate mixed rarified continuum flows. Refer to a companion paper and presentation [10] for an overview of the PSI Project PSC Element which further describes the role of rarefied flow in PSI.

A. History of the Boltzmann Application

Beginning in 2012, NASA/MSFC evaluated a hybrid method that coupled the solution of the Navier-Stokes equations using traditional methods with the Boltzmann equations solved by the discrete velocity method (DVM)[6]. The coupling is accomplished by choosing cell-by-cell which governing equations to solve based on a continuum breakdown criteria (CBC) which is similar to a Knudsen number criteria. As the solution progresses, the balance of cells for each approach is changed based on the evolution of the CBC. The application which implemented this approach, termed here as Boltzmann, was developed by CFDRC, Inc since 2005 [11]. In 2016, the DVM approach was implemented [12] in the Loci framework and coupled with the Loci/Chem CFD application. The Loci/Chem-Boltzmann application is theoretically capable of solving the coupled Navier-Stokes and Boltzmann equations for the PSI application. At the start of the PSI Project, the Loci/Chem-Boltzmann application was at a proof of concept state.

B. Initial assessment of Loci/Chem-Boltzmann for PSI

At the beginning of the PSI Project, the Loci/Chem-Boltzmann application was assessed for capability by constructing a simulation of the Apollo Lunar Excursion Module (LEM) at 5 meters elevation above the Lunar surface. See Fig. 1 in which the soil is depicted by the purple shaded region. The 23 million cell, unstructured computational mesh includes resolution of turbulent boundary layers on the Lunar surface and all vehicle surfaces.

The plume effluent was modeled using Argon since the Loci/Chem-Boltzmann application was limited to monoatomic gases at that time. Significant difficulties were encountered in conducting the simulation. The greatest of these difficulties arose from the significant memory requirements of the DVM solution. The memory use of the Boltzmann DVM solver can require 5,000 times greater memory per cell than the Navier Stokes solution for practical PSI applications using a 30X30X30 velocity space discretization [13]. Although the computational effort to conduct the DVM is also commensurately greater than the Navier-Stokes solution, unless the memory is balanced very carefully in a highly parallel supercomputer simulation, memory is exhausted on a CPU core and the simulation fails. The initial memory balancing implementation of the Loci/Chem-Boltzmann application at this time could not support the requirements of simulating the Apollo LEM demonstration simulation.

Although the ability to complete the demonstration simulation was not demonstrated, several important accomplishments were achieved for the practical PSI demonstration. A few notable accomplishments were: i) execution on practical size computational meshes, ii) successful re-partitioning of computational cells between the Navier-Stokes and Boltzmann solution methods, iii) iterative convergence of coupled Navier-Stokes and Boltzmann equations at the timestep level, and iv) convergence of the solution in time at a given partition of Navier-Stokes and Boltzmann allocated cells. An implication of the demonstration was that simulation of practical, manned-scale, Lunar landers PSI is an achievable objective.

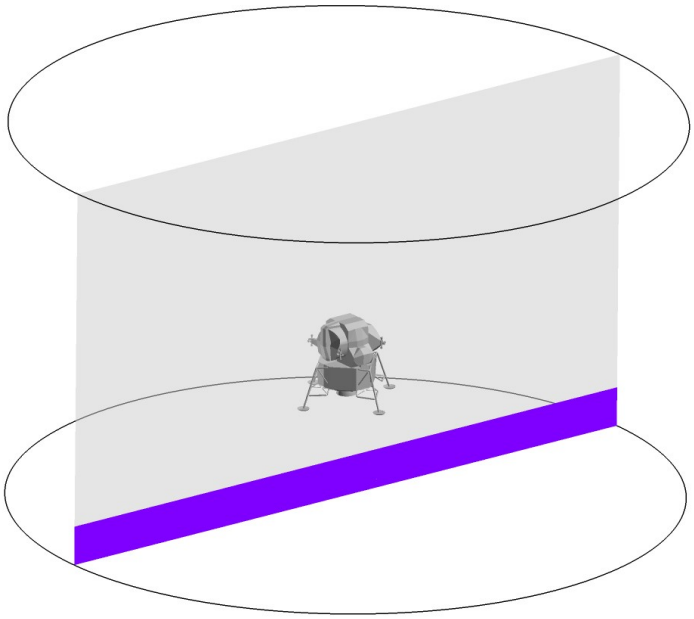


Fig. 19 Depiction of the CFD simulation of the Apollo LEM at an altitude of 5 meters above the Lunar surface. A layer of Lunar soil is depicted by the purple shaded region.

C. Loci/Chem-Boltzmann Development Activities

During the first year of the PSI Project, the Loci/Chem-Boltzmann DVM solver was augmented with the implementation of the Bhatnagar–Gross–Krook (BGK) and Shakov models [13] of the intermolecular collisions term of the Boltzmann equation. These models were introduced to reduce the computational effort required to conduct the DVM solution. These methods were verified and validated using data from unit physics experiments. In addition, steps began to extend the plume effluent modeling capability towards a realistic measure of actual rocket exhaust products with the implementation of diatomic gas models. Research began into developing methods, ranging from multiple species gas mixture models to equivalent species representation of mixtures of gases.

The significant barriers to production use of Loci/Chem-Boltzmann application, described in the previous subsection, were addressed. Significant development work was accomplished in extending the Loci framework [14] to balance both memory and computational effort. The time required for writing the hybrid flowfield to disk, including the velocity space for each Boltzmann equation cell, was also found to be prohibitive. A parallel I/O implementation using the feature of the Lustre filesystem [15] on the NAS Pleiades supercomputer was implemented to address this performance detriment.

D. Current Assessment of the Loci/Chem-Boltzmann Application

After significant development work the Apollo LEM simulation was revisited again using Argon as the plume effluent. The unstructured mesh distribution is shown in Fig. 20, in which mesh is clustered around the Apollo LEM and descent engine nozzle bell for a total of 23 million cells. Approximately 4200 cpu cores of the NAS Pleiades supercomputer were used to perform this simulation. The simulation was conducted by using a Navier-Stokes solution as an initial condition generated by Loci/Chem. The initial condition solution is shown in Fig. 21. Static temperature contours are shown on the left and velocity magnitude on the right. The Log base ten pressure on the Lunar surface is shown in grayscale. Note the expansion of the descent engine plume and the upward flow from the base of the LEM around the vehicle and towards the farfield, which creates wakes behind LEM geometric protrusions.

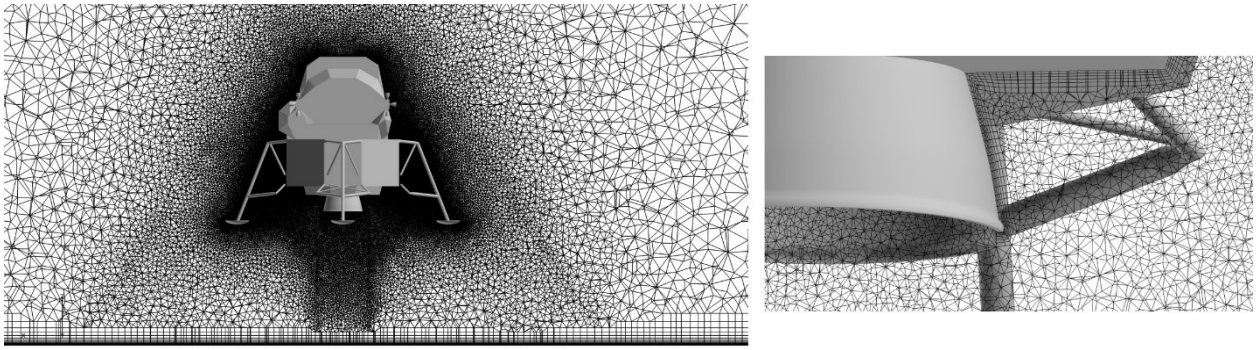


Fig. 20 Computational mesh used for the CFD simulation of the Apollo LEM at an altitude of 5 meters above the Lunar surface. Note clustering of mesh resolution and boundary layer mesh near vehicle and descent engine nozzle bell.

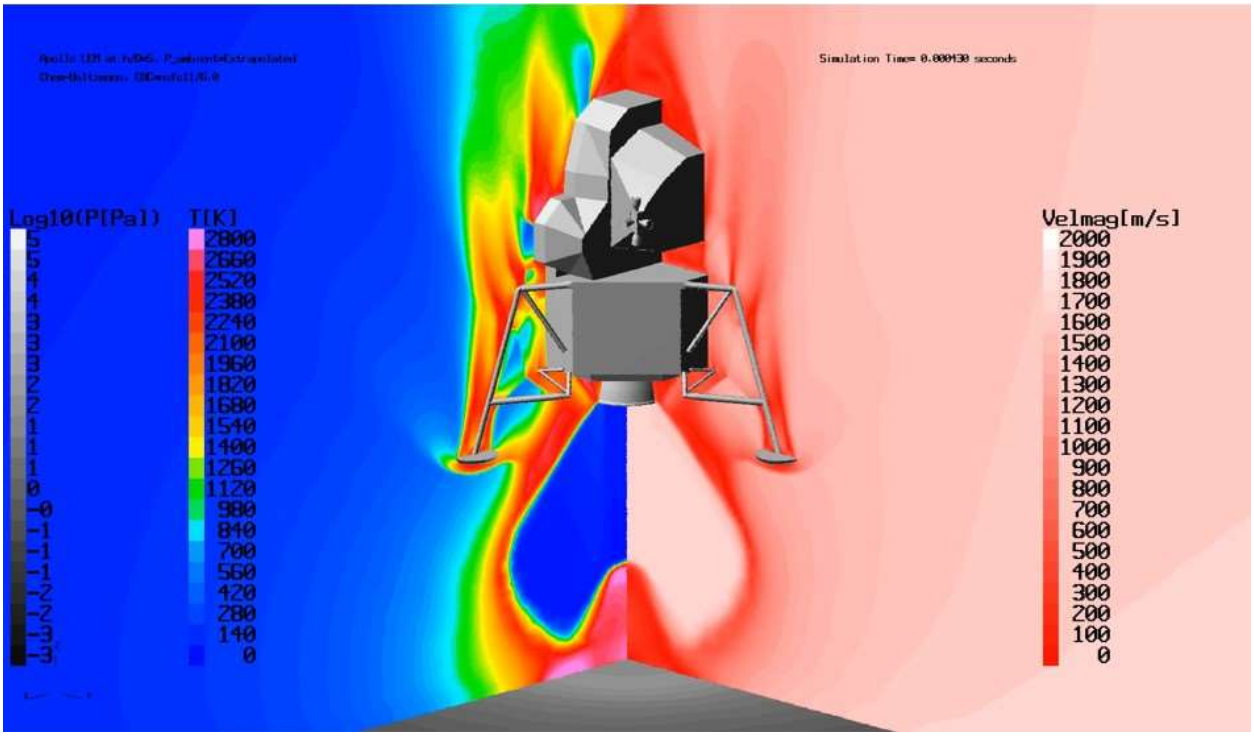


Fig. 21 Initial condition for the Loci/Chem-Boltzmann simulation conducted using only the Navier-Stokes equations. Static temperature contours are shown on the left and velocity magnitude on the right. The Log base ten pressure on the Lunar surface is shown in grayscale.

The continuum breakdown criteria (CBC), shown in Eq. 1, is a measure which, like the Knudsen number, indicates the degree of rarefaction of the flow. Note that variations in flow field static pressure, p, and velocity, V, result in length scales which are weighed relative to the mean free path, λ.

$$CBC = \lambda\sqrt{\left(\frac{\nabla p}{p}\right)^2 + \frac{tr[(\nabla V)^T(\nabla V)]}{V^2}} \tag{1}$$

For this example, the criterion was set to activate the use of Boltzmann cells at CBC values above 6. The resulting distribution of Navier-Stokes and Boltzmann cells is shown in Fig. 22 below. The cells in which the Boltzmann equation is solved are those shaded in blue. Note the CBC activates near the descent engine exit and expansion surface as well as just upstream and in the wakes of geometric protrusions from the Apollo LEM surface. When using this relatively high value of the CBC to activate the Boltzmann solver, the region near the Lunar surface is not activated. In reality, the boundary layer near the ground is expected to contain high gradients and some degree of rarefaction, requiring Boltzmann solver treatment for an accurate solution. However, decreasing the CBC to low enough values to activate this treatment near the Lunar surface would result in intractably large numbers of Boltzmann cells in portions of the domain with negligible effect on PSI phenomena (such as the wake regions with Boltzmann cells in this demonstration). The number of Boltzmann cells required for the demonstration simulation was 7.1 million cells, or 30 percent of the total computational cells. Future development may allow zonal restriction of the CBC, such that Boltzmann cells will be used only in regions of high gradients, rarefaction, and importance to the physics of interest for the problem at hand. For example, in this case, the near-ground region will have a first order effect on PSI. An explicit zonal restriction for the CBC could allow a lower value, activating some Boltzmann cells near the surface, while ignoring the large wake above the vehicle, and keeping the total number of Boltzmann cells within computational limitations.

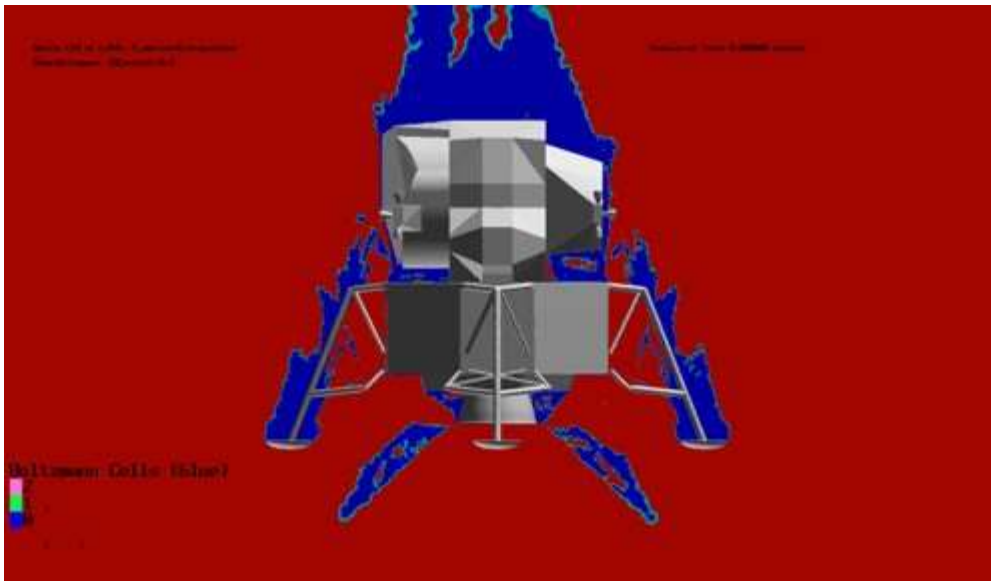


Fig. 22 Distribution of Navier-Stokes and Boltzmann cells in the Apollo LEM simulation. Boltzmann cell locations are those regions shaded in blue.

The timestep used in the hybrid unsteady simulation was 0.3 microseconds. The number of Newton sub-iterations used was 5. The simulation was conducted for a total simulation time of 6 milliseconds during a wall-clock elapsed time of 20 days. The number of Boltzmann cells began at several million and quickly converged to the 7.1 million value mentioned in the previous paragraph. The distribution of memory over the parallel simulation was observed to maintain balance within about 10 percent during the entire simulation, confirming the resolution of this issue identified in the previous assessment. The time required for reading the initial conditions from file as well as writing the final solution to file was greatly reduced from that observed during the initial assessment. Currently, these file I/O events take from five to ten minutes each, not a negligible amount of time but not prohibitive to conducting the simulation.

Points within the Boltzmann regions were probed to track the solution progression as a function of time. An example of the pressure and temperatures at these locations are shown in Fig. 23. These values change significantly at early time and then approach convergence as the simulation progresses. Error residuals dropped by approximately one to three orders of magnitude for each timestep during the simulation. No robustness issues were encountered during the simulation.

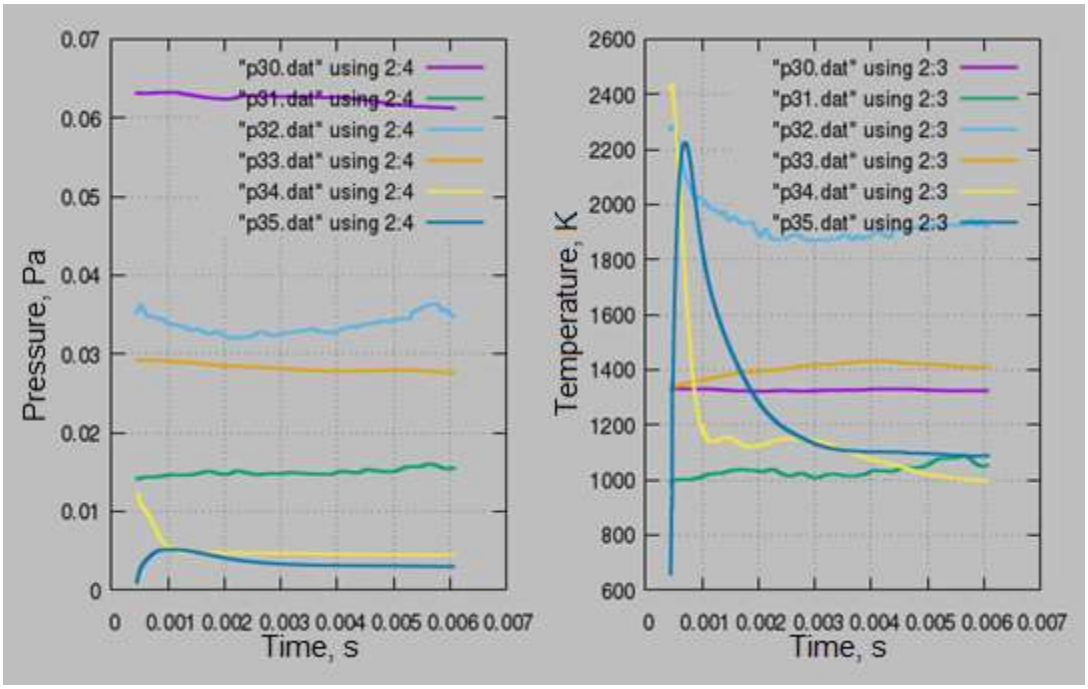


Fig. 23 Static pressure (left) and static temperature (right) as a function of time at probe locations within the Boltzmann equation regions. Each color represents a different probe location.

E. Summary of Activities and Accomplishments

The assessment of the ability to use the Loci/Chem-Boltzmann application for practical PSI simulation has produced a positive outcome. With continued refinement, it is expected that hybrid applications such as Loci/Chem-Boltzmann will be capable of performing simulations of PSI effects of manned Lunar landers at a resolution level and timeframe suitable for assessment of PSI risk to the mission. Ongoing efforts are focused on developing an equivalent gas model of plume effluent and continuing to improve performance and robustness. Efforts have been started to couple the Boltzmann solver with the two-phase gas/soil Loci/GGFS application, which simulates the soil erosion and cratering due to plume impingement on soil surfaces in low ambient pressure.

The success of the assessment presented above enables the beginning of validation efforts for the Loci/Chem-Boltzmann application. The PSC validation plan defines the dataset of Legge [16] for this purpose. This subscale experiment measured plume impingement pressure and impingement surface shear stress for supersonic plumes impinging on a solid surface in very low ambient pressure. The dataset includes a range of conditions covering the transition from continuum to rarefied flow effects on the solid surface shear stress. Accurately capturing the effects of this transition will be a key part of validating Loci/Chem-Boltzmann for use in simulating PSI relevant plumes at very low pressure.

V.Conclusion

Existing toolsets have potential application in simulating PSI phenomena. The Loci/Chem tool has been used extensively and validated for simulating rocket plumes in Earth atmosphere. The present work shows that this tool can also be validated for simulating plumes in Martian atmosphere, and a baseline validation assessment for such use has already been completed. A more rigorous detailed assessment has been started, and results to date indicate Loci/Chem is likely capable of achieving threshold performance for predicting plume flows in Martian environments without additional development. The Loci/Chem-Boltzmann tool is under active development. The present work indicates that this tool has application in simulating plumes in extreme rarefied Lunar atmosphere. A simulation of the Apollo LEM near the lunar surface has demonstrated that development efforts to date have been effective at achieving production capability for this tool. A validation assessment can now be made to evaluate the accuracy of Loci/Chem-Boltzmann predictions of plumes in Lunar environments. Ongoing developments are expected to further improve performance and accuracy during validation efforts.

References

[1] West, J. S., “Game Changing Development Program: Plume Surface interaction Predictive Simulation Capability: Validation Plan”, NASA, Nov. 2021.

[2] Luke, E., “A Rule-Based Specification System for Computational Fluid Dynamics,” Ph.D. Dissertation, Mississippi State University, Dec. 1999.

[3] Luke, E., and George, T., “Loci: A Rule-Based Framework for Parallel Multidisciplinary Simulation Synthesis,” Journal of Functional Programming, Special Issue on Functional Approaches to High-Performance Parallel Programming, Volume 15, Issue 03, 2005, pp. 477-502.

[4] Veluri, S. P., Roy, C. J., Hebert, S., and Luke, E. A., “Verification of the Loci/Chem CFD Code using the method of Manufactured Solutions,” *46th AIAA Aerospace Sciences Meeting and Exhibit*, Jan. 2008, pp. 661.

[5] Roy, C., Eric, T., Veluri, S., Rifki, R., Luke, E., and Hebert, S., "Verification of rans turbulence models in Loci/Chem using the method of manufactured solutions.” *18th AIAA Computational Fluid Dynamics Conference*, 2007, p. 4203.

[6] Harris, R. E. and Turansky, C. P., “Validation of Boltzmann discrete velocity method flow solver for diatomic gases and multi-component monatomic gas mixtures,” *AIAA Scitech 2020 Forum,* 2020, p. 2154.

[7] Inman, J., “Fluorescence Imaging Study of Free and Impinging Supersonic Jets: Jet Structure and Turbulent Transition,” Ph.D. Dissertation, The College of William and Mary in Virginia, 2007.

[8] Shurtz, T.P., “Initial Loci-CHEM Simulations of Under-expanded Jets in Mars-like Ambient Pressure”, Jacobs Space Exploration Group Memo JPID-FY20-001819, 2021.

[9] Danehy, P. M., Palma, P. C., McIntyre, T. J., and Houwing, A. F. P., "Comparison of theoretical laser-induced fluorescence images with measurements performed in a hypersonic shock tunnel", AIAA Paper 96-2236, 1996.

[10] West, J. S., and Liever, P. A., “Overview of the Predictive Simulation Capability Element of the Plume Surface Interaction Project”, SciTech 2022, Paper 3609962, January, 2022.

[11] Various Authors, Development of the Unified Flow Solver, NASA STTR contracts NNK08EB52C, NNX10CB66C and NNX14CK11C.

[12] Harris, R. E., “Development of Coupled Rarefied/Continuum Gas Solver in the Loci Framework”, NASA STTR Phase III final report, contract NNM15AE00P, 2015.

[13] Harris, R., E., “Introduction to Boltzmann Equation and Discrete Velocity Method”, Presentation to the PSI Project Predictive Simulation Capability Weekly forum, NASA/MSFC, 2 Feb. 2021.

[14] E. Luke and T. George, "Loci: A Rule-Based Framework for Parallel Multidisciplinary Simulation Synthesis," Journal of Functional Programming, vol. 15, no. 3, pp. 477-502, 2005.

[15] NASA High End Computing Program, “Pleiades Lustre Filesystems”, https://www.nas.nasa.gov/hecc/support/kb/pleiades-lustre-filesystems_225.html, 2021.

[16] Legge, H., “Plume Impingement Forces on Inclined Flat Plates”, Rarefied Gas Dynamics, VCH Press, Weinheim, Germany, 1991, pp. 955-962.